# Time-Resolved Resonance Raman and Time-Resolved Step-Scan FTIR Studies of Nitric Oxide Reductase from *Paracoccus denitrificans*: Comparison of the Heme $b_3$-$Fe_B$ Site to That of the Heme-$Cu_B$ in Oxidases[†]

Eftychia Pinakoulaki and Constantinos Varotsis*

*Department of Chemistry, University of Crete, 71409 Heraklion, Crete, Greece*

*Received July 22, 2003; Revised Manuscript Received October 22, 2003*

ABSTRACT: Time-resolved resonance Raman ($TR^3$) and time-resolved step-scan ($TRS^2$) FTIR spectroscopies have been used to probe the structural dynamics at the heme $b_3$ proximal and distal sites after carbon monoxide photolysis from fully reduced CO-bound nitric oxide reductase. The Raman spectra of the transient species exhibit structural differences relative to the equilibrium geometry of heme $b_3$. The most significant of these is a shift of 8 $cm^{-1}$ to higher frequency of the 207 $cm^{-1}$ mode, and a shift of 7 $cm^{-1}$ to lower frequency of the $\nu_4$ mode. Our results indicate that the 207 $cm^{-1}$ mode observed in the equilibrium-reduced heme $b_3$ originates from $\nu$(Fe−His). Its behavior in the photolytic transients indicates that the relaxed Fe−His state is not significantly populated. We suggest that relaxation along the tilt angle ($\theta$) of the proximal histidine with respect to the heme plane and the out-of-plane displacement of the Fe ($q$) are coupled, and ligand binding and dissociation are accompanied by significant changes in the angular orientation of the His ligand. The results are compared to those obtained for the $aa_3$-cytochrome *c* oxidase from *Paracoccus denitrificans*. The results are compared to those obtained for the $aa_3$-cytochrome *c* oxidase from *P. denitrificans*. The $TR^3$ and $TRS^2$ FTIR data demonstrate significant alterations in the nature of the heme-protein dynamics between nitric oxide reductase and heme-copper oxidases resulting from specific structural differences in their respective hemepockets.

The bacterial nitric oxide reductase (NOR)[1] is a membrane protein that forms the N−N bond during denitrification (*1*−*4*). NOR from *Paracoccus denitrificans* is purified as a two-subunit complex NorBC (*1*). The smaller subunit (NorC) is a membrane bound cytochrome *c*. NorB is homologous to subunit I of heme-copper oxidases, and contains a low-spin heme *b* and a dinuclear high-spin heme $b_3$/non-heme $Fe_B$ center, where NO binding and reduction to $N_2O$ takes place (*1*−*4*). Substantial progress has been made recently in gaining a molecular level of understanding the structural similarities between heme-copper oxidases and bacterial NO reductases because some heme-copper oxidases and NOR reduce both NO and $O_2$ (*1*−*5*). For better understanding of the structure−function relationship of NOR and heme-copper oxidases, it is highly desirable to elucidate the differences associated with ligand dynamics among these proteins.

In the absence of a crystal structure of NOR, the structural interpretation of spectroscopic data for ligand binding is based solely on comparisons with the structures of 6-coordinate heme protein−ligand adducts, models, and heme-copper oxidases. The resonance Raman (RR) spectrum of oxidized NOR shows two distinct $\nu_{as}$(Fe−O−Fe) modes at 813 and 833 $cm^{-1}$ that have been attributed to two different conformations (*open* and *closed*) of the catalytic site of the enzyme (*3*). The ferric nitrosyl complex of NOR, bearing a strong resemblance to the corresponding derivative of hemoglobin and myoglobin, has also been characterized by its $\nu(Fe^{3+}$-NO) and $\nu$(N−O) at 594 and 1904 $cm^{-1}$, respectively (*3*). Furthermore, it has been shown from RR studies that the frequencies of the Fe−C−O are quite different in NOR as compared with heme-copper oxidases (*2*). On the basis of these observations, it has been proposed that the catalytic heme $b_3$ is present in a negatively charged environment, in which CO adopts a unique geometry. The rate of CO recombination ($k_{obs} = 2 \times 10^5$ $s^{-1}$, [CO] = 1 mM) to heme $b_3$ has also been reported, but detailed structural information of the dinuclear center was difficult to infer from the transient optical absorption studies (*4*). Moreover, low-temperature (light-dark) FTIR experiments have revealed that upon photodissociation of CO from heme $b_3$, the $Fe_B$-CO complex is formed (*1*).

Of the spectroscopic methods available for characterization of the dynamics of heme protein active sites, time-resolved resonance Raman spectroscopy ($TR^3$) is a powerful technique because excitation within the heme $\pi-\pi^*$ electronic absorption transitions selectively enhances vibrational modes of the heme and bound- proximal/distal ligands without the interference from the modes associated with the protein matrix (*6*−*11*). On the other hand, time-resolved step-scan ($TRS^2$) FTIR difference spectroscopy has the sensitivity and resolution to detect, in addition to ligands bound to metal centers in a protein, structural changes within the protein (*12*). $TR^3$,

[†] This work was partially supported from the Greek Ministry of Education.

* Corresponding author. E-mail: varotsis@edu.uoc.gr. Fax: +30−2810−393601. Tel: +30−2810−393653.

[1] Abbreviations: NOR, nitric oxide reductase; CcO, cytochrome *c* oxidase; RR, resonance Raman; $TR^3$, time-resolved resonance Raman; $TRS^2$-FTIR, time-resolved step-scan Fourier transform infrared.

10.1021/bi035289m CCC: $25.00 
Published on Web 11/22/2003

time-resolved IR, and TRS$^2$ FTIR have been applied to heme-copper oxidases to measure conformational and structural changes, as well as kinetic properties of transient species (*6*−*10*, *13*−*14*, *12*, *15*−*17*). The TR$^3$ studies have demonstrated that the photolytic transient species, when compared to the equilibrium unligated species, provide information on the actual molecular changes that occur in the heme protein (*6*−*11*). Changes in the heme vibrational frequencies in the CO photoproduct relative to the equilibrium deoxy protein, in particular the $\nu_4$ ($C_a$-N) and the Fe−His stretching vibrations, have been used to gain insight in the dynamics of heme proteins. Vibronic theory applications have revealed that both the tilt angle ($\theta$) of the proximal histidine with respect to the heme plane, and the out-of-plane displacement of the Fe ($q$) are the critical coordinates in the dynamics of heme protein relaxation (*18*−*19*).

In the work presented here, we have used both TR$^3$ and TRS$^2$ FTIR spectroscopies to characterize the heme pocket dynamics of fully reduced NOR after CO photolysis. We also compare the FTIR and TRS$^2$ FTIR spectra of the CO-bound NOR and $aa_3$-cytochrome *c* oxidase (CcO) from *P. denitrificans* at room temperature. The TR$^3$ spectra of the transient species exhibit structural differences relative to the equilibrium geometry of heme $b_3$. The most significant of these is a shift of 8 cm$^{-1}$ to higher frequency of the 207 cm$^{-1}$ mode, originating from $\nu$(Fe−His), and a shift of 7 cm$^{-1}$ to lower frequency of the $\nu_4$ mode. The relative rates of CO recombination and photoproduct relaxation indicate that the relaxed Fe−His state is not significantly populated, and only the mode associated with the transient Fe−His state is observed. We suggest that relaxation along $q$ and $\theta$ are coupled, and ligand binding and dissociation are accompanied by significant changes in the angular orientation of the His ligand. The combination of the TR$^3$ and TRS$^2$ FTIR results suggests significant alterations in the nature of the heme-protein dynamics between NOR and cytochrome *c* oxidase.

## MATERIALS AND METHODS

NOR was purified from *P. denitrificans* according to published procedures (*1*). The activity of the enzyme was 40 $\mu$mol mg$^{-1}$ min$^{-1}$ (46e$^-$/s). The samples were concentrated to 150 $\mu$M in 20 mM Tris pH 7.4 containing 0.05% dodecyl $\beta$-D-maltoside and stored in liquid nitrogen until use. The concentration of NOR was determined using $\epsilon_{411} = 3.11 \times 10^5$ M$^{-1}$ cm$^{-1}$. The $aa_3$-cytochrome *c* oxidase from *P. denitrificans* was isolated according to published procedures (*20*). The TR$^3$ spectra were acquired as described elsewhere (*8*, *10*). For CO photolysis, the pump laser was used at 532 nm with 1.1 mJ/pulse. The probe laser was used at 416 nm with 0.5 mJ/pulse. Approximately 40 $\mu$L of a 50 $\mu$M dithionite-reduced samples were placed in a rotating quartz Raman cell to minimize local heating and exposed to 1 atm CO. The Raman sample cells are custom designed for anaerobic measurements and can be used for recording both the resonance Raman and optical absorption spectra (Perkin-Elmer Lamda 20 UV−visible spectrometer). The pD solutions prepared in $D_2O$ buffers were measured by using a pH meter and assuming pD = pH (observed) + 0.4. FTIR spectra were obtained with a Bruker Equinox 55 FTIR spectrometer equipped with liquid nitrogen cooled mercury cadmium telluride (MCT) detector. Dithionite reduced samples (400−500 $\mu$M) were exposed to 1 atm CO (1 mM) in an anaerobic cell to prepare the carbonmonoxy adduct, and loaded anaerobically into a cell with $CaF_2$ windows and a 0.025 mm spacer samples. The FTIR spectra were obtained as a difference, using the buffer as background, and each spectrum is the average of 1000 scans. The spectral resolution used for the static FTIR measurements was 4 cm$^{-1}$. In the TRS$^2$ FTIR experiments the 532 nm pulse from a Continuum Nd:YAG laser (7-ns width, 3 Hz) was used as a pump light (5−10 mJ/pulse) to photolyze the CO-bound NOR and CcO enzymes. The TRS$^2$ FTIR spectra were obtained with 8 cm$^{-1}$ spectral resolution and 5 $\mu$s time resolution for the 5 $\mu$s to 4 ms measurements or 100 $\mu$s resolution for the 100 $\mu$s to 80 ms measurements. Ten coadditions per retardation data point were collected, and 2−3 measurements were averaged. Changes in intensity were recorded with an MCT detector, amplified (dc-coupled), and digitized with a 200- kHz, 16-bit, analog-to-digital converter. Blackman-Harris three-term apodization with 32 cm$^{-1}$ phase resolution and the Mertz phase correction algorithm were used. Difference spectra were calculated as $\Delta A = -\log(I_S/I_R)$. The rate constant for the CO rebinding to heme $a_3$ was calculated with a three-parameter exponential fit to the experimental data. Optical absorbance spectra were recorded before and after FTIR measurements to assess sample stability with a Perkin-Elmer Lamda 20 UV−visible -spectrometer.

## RESULTS AND DISCUSSION

*A. Optical Absorption Spectra of NOR and $aa_3$ Cytochrome c Oxidase from P. denitrificans.* The optical absorption spectra of oxidized, reduced, and CO-bound-reduced NOR are shown in Figure 1A. The difference CO-bound-reduced spectrum, shown in the inset, displays a positive band at 419 nm with a trough at 434 nm. The optical data are in agreement with earlier observations (*4*, *21*). The optical absorption spectra of oxidized, reduced, and CO-bound-reduced $aa_3$ are shown in Figure 1B. The difference spectrum (reduced-CO minus reduced), shown in the inset, displays maxima and minima at 430 and 447 nm, in agreement with that previously reported (*22*).

*B. TR$^3$ of NOR.* The high-frequency TR$^3$ spectra of NOR at various delay times ($t_d$ = 10 ns to 1 ms) after CO photolysis in the 1200−1700 cm$^{-1}$ region are shown in Figure 2A, and are compared to that of the equilibrium reduced enzyme (trace a). Trace b is the spectrum of CO-bound reduced NOR. In the spectrum of the equilibrium reduced enzyme, the oxidation state marker, $\nu_4$, is located at 1362 cm$^{-1}$, characteristic of hemes *b*/*c* and $b_3$ in their ferrous states (*2*, *3*). The $\nu_2$ bands are located at 1560 (heme $b_3$) and at 1584/1591 cm$^{-1}$ (heme *b*/*c*). The core-sensitive bands $\nu_3$ are located at 1472 cm$^{-1}$ (five-coordinate heme $b_3$) and at 1494 cm$^{-1}$ (six-coordinate heme *b*/*c*). This indicates that heme $b_3$ is 5-coordinate in the ferrous state and the initial binding of CO to reduced heme $b_3$, in contrast to previous reports (*4*), does not require the displacement of an endogenous distal ligand of heme $b_3$. Upon addition of CO to reduced NOR, the appearance of the $\nu_4$ vibration at 1371 cm$^{-1}$ as well as the loss of the $\nu_3$ intensity of the high spin heme $b_3$ indicates CO binding (trace b). In the spectra of the photolytic transients obtained at $t_d$ = 10 ns to 1 ms after CO photolysis, the $\nu_4$ and $\nu_3$ modes of heme $b_3$ display frequency and/or intensity changes relative to the equilibrium

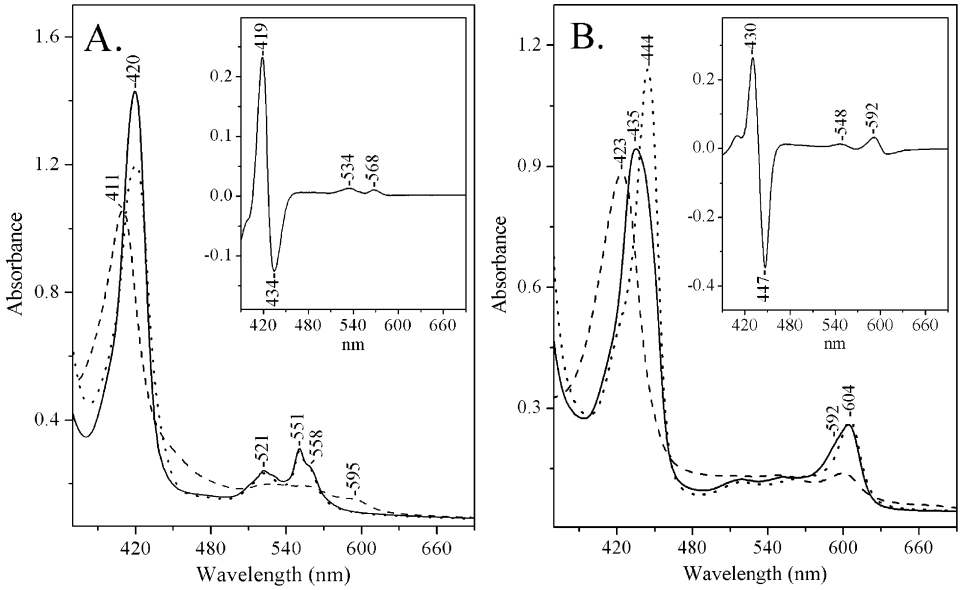


FIGURE 1: (A) The optical absorption spectra of oxidized (dashed line), dithionite reduced (dotted line), and CO-bound NOR (solid line). The difference optical spectrum of CO-bound *minus* dithionite reduced NOR is depicted in the inset. (B) The optical absorption spectra of oxidized (dashed line) dithionite reduced (dotted line) and CO-bound $aa_3$ from *P. denitrificans* (solid line). The difference optical spectrum of CO-bound *minus* dithionite reduced $aa_3$ is depicted in the inset.

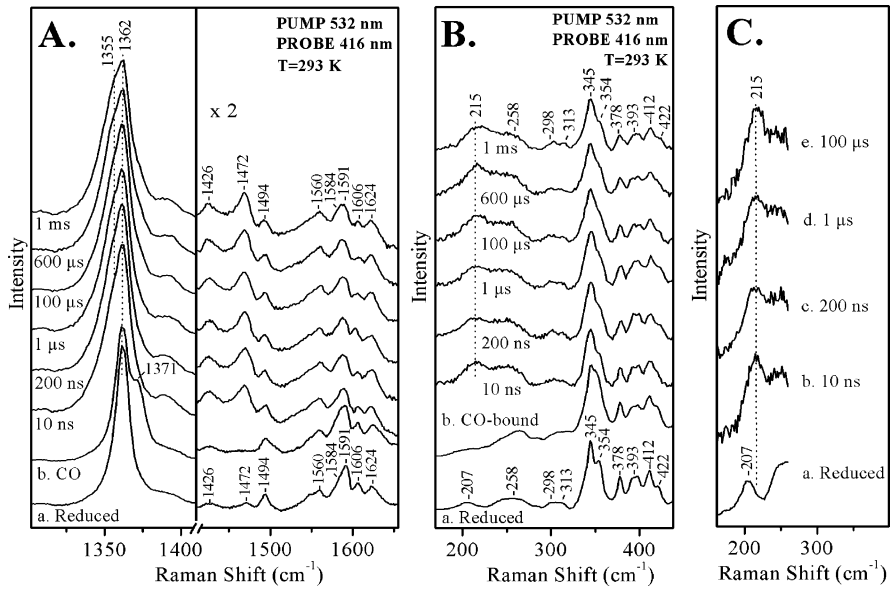


FIGURE 2: (A) High-frequency time-resolved resonance Raman ($TR^3$) spectra of fully reduced NOR at the indicated times after CO photolysis. The energy of the 532-nm photolysis pump/pulse was 1.1 mJ, sufficient to photolyze the NOR−CO complex. The energy of the 416-nm probe beam was 0.5 mJ/pulse. The repetition rate for both the pump and probe beam was 10 Hz. The accumulation time was 15 min for all spectra. The equilibrium fully reduced (trace a) and CO-bound forms of NOR (trace b) were obtained with 413.1 nm excitation from a Krypton ion laser. (B) Low-frequency $TR^3$ spectra of fully reduced NOR at the indicated times after CO photolysis. All other conditions were the same as for Figure 1A. (C) Expanded region of the Fe−His mode.

species. The $\nu_4$ mode displays a shift to lower frequency, indicating increased porphyrin $\pi^*$ electron density relative to the equilibrium species. We suggest that the noticeable intensity increase of the $\nu_3$ band is due to the higher Raman cross section in the photoproduct than in the equilibrium species and in the CO-bound form. The absence of a shift to lower frequency of the $\nu_3$ band, as it was observed in heme $a_3$ of CcO (*6*−*9*), indicates that upon CO photolysis the heme $b_3$ core does not expand. The behavior of both the $\nu_4$ and $\nu_3$ modes strongly resembles that found in the transient spectra of various hemoglobins (*11*) but is different from that observed in heme $a_3$ of CcO (*6*−*9*) and in heme $o_3$ of cytochrome $bo_3$ (*10*).

The low-frequency region of the $TR^3$ spectra is shown in Figure 2B. The spectra of the equilibrium fully reduced and CO-bound NOR are shown in traces a and b, respectively. The only frequency change upon photodissociation of CO occurs in the 207 cm$^{-1}$ mode. In addition, a significant intensity change is observed in the 354 cm$^{-1}$ mode. Therefore, these modes can be assigned to reduced heme $b_3$. Figure 2C shows an expansion of the Fe−His stretching mode in the transient spectra. The five-coordinate, high-spin, histidine ligated heme $b_3^{+2}$ should exhibit the Fe−His stretching vibration in the 200−260 cm$^{-1}$ region, with its value reflecting the extent of anionic character present on the His. In globins and CcO, in which the His is neutral,

this mode occurs between 200 and 230 $cm^{-1}$ and is dependent on the extent of H-bonding to the histidine N−H (*23*). For peroxidases, with a strongly basic His, the $\nu$(Fe−$His^-$) occurs in the 240−260 $cm^{-1}$ region (*23*). Consistent with its assignment as originating from Fe−His, the 207 $cm^{-1}$ mode is not present in the spectrum of oxidized enzyme (*3*) nor in the spectrum of the CO-bound enzyme. The frequency we observe at 207 $cm^{-1}$ indicates the Fe−His mode is not H-bonded. If a H-bond were to form, we would expect to see the Fe−His near 220 $cm^{-1}$ (*23*). The 207 $cm^{-1}$ mode in the reduced enzyme shifts to 215 $cm^{-1}$ in the photoproduct ($t_d$ = 10 ns). Similar transient Fe−His behavior was originally noted for Hb (*11*), mammalian CcO (*6*−*9*), and cytochrome $bo_3$ (*10*). It is worth noting that such frequency shift of the Fe−His mode has been also observed after photolysis of $O_2$ from the heme $a_3$ of CcO during the CcO/$O_2$ reaction (*7*). The $\nu$($Fe^{2+}$-His) is essentially unchanged relative to its original position in the photoproduct during the entire dynamic process (10 ns to 1 ms). This results from the CO photolysis by the probe 416 nm beam, producing the 10-ns spectrum. Combining the results above with those previously reported (*4*, *21*) on the rate of CO recombination ($k_{obs}$ = (2−3) × $10^5$ $s^{-1}$) we suggest that the rate of photoproduct relaxation is similar to the rate of CO rebinding. This way, the relaxed Fe(II)-His state is not significantly populated and only the mode associated with the transient Fe(II)-His* state is observed in the $TR^3$ experiments.

The $\nu$($Fe^{2+}$-His) frequency has been proposed to be inversely related to the out-of-plane distance of the heme Fe (*18*−*19*). The upshift in $\nu$($Fe^{2+}$-His) of heme $b_3$ after CO photolysis suggests that the iron is closer to the heme plane in the photoproduct than in the equilibrium deoxy form, and that CO binding moves the iron more into the heme plane. Changes in $\theta$ introduces $\sigma$(Fe−$N_{His}$)-$e_g$($\pi$*) mixing, that populates the $e_g$($\pi$*) antibonding orbital and affects the $\nu_4$ (*18*−*19*). This is also the situation in heme $b_3$ ($\nu_4$ = 1355 $cm^{-1}$). On the other hand, the out-of-plane displacement ($q$) mixes both $a_{1g}(d_z^2)/a_{2u}(\pi)$ and $\sigma$(Fe−$N_{His}$)/$a_{2u}$($\pi$) and affects primarily the resonance enhancement and frequency of the $\nu$($Fe^{2+}$-His) mode. If relaxation along $q$ and $\theta$ are coupled, then correlation between $\nu_4$ and $\nu$(Fe−His) is expected (*18*−*19*). The relaxation along the out-of-plane coordinate dominates when the changes along the tilt coordinate are small, and no a priori correlation between the $\nu_4$ and $\nu$($Fe^{2+}$-His) is predicted. This appears to be the situation in heme $a_3$ (*6*) and heme $o_3$[2] (*10*) relaxation suggesting that ligand binding and dissociation are not accompanied by significant changes in the angular orientation of the histidine ligand. The correlation that occurs between $\nu_4$ and $\nu$($Fe^{2+}$-His) in NOR is similar to that of Hb·CO photolysis (*11*), but distinctly different from that found in heme-copper oxidases (*6*−*10*). Therefore, heme $b_3$ relaxation in NOR occurs along $q$ and $\theta$, and ligand binding and dissociation are accompanied by significant changes in the angular orientation of the histidine ligand.

*C. FTIR and TRS[2] FTIR of NOR and Cytochrome $aa_3$ from P. denitrificans.* Figure 3A,B show the FTIR spectra of CO-bound NOR and $TRS^2$ FTIR difference spectra after CO photolysis, respectively, at room temperature. For comparison, the fully reduced $aa_3$−CO complex of the *P. denitrificans* enzyme is included (Figure 3C,D). Figure 3A (traces a and c) demonstrates that the C−O stretching mode of NOR

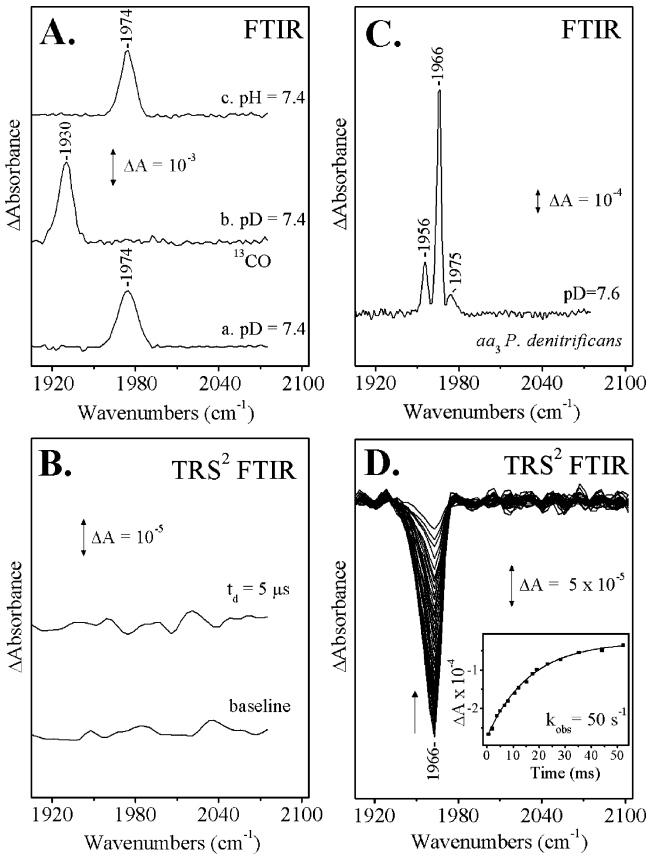


FIGURE 3: (A) FTIR spectra of the fully reduced CO-bound NOR at pD 7.4 (trace a), NOR-$^{13}$CO, pD 7.4 (trace b), and pH 7.4 (trace c). (B) Time-resolved step-scan ($TRS^2$) FTIR difference spectrum of the fully reduced CO-bound NOR at 5 $\mu$s after CO photolysis. The spectrum at 5 $\mu$s before the laser fire is included as baseline. A 532 nm pump beam (5−10 mJ/pulse) at a repetition rate of 3 Hz was used for photolysis. The spectral resolution was 8 $cm^{-1}$. (C) FTIR spectra of the fully reduced CO-bound cytochrome $aa_3$ from *P. denitrificans* at pD 7.6. (D) $TRS^2$ FTIR difference spectra of the fully reduced CO-bound cytochrome $aa_3$ at 5 $\mu$s to 50 ms after CO photolysis. The time resolution was 5 $\mu$s for the 5 $\mu$s to 4 ms data points and 100 $\mu$s for the 4−50 ms data points. Other conditions were the same as for Figure 2B. Inset: Plot of the $\nu$(FeC−O) mode versus time after CO photolysis.

is located at 1974 $cm^{-1}$, and is insensitive to H/D exchange. The $^{13}$C−O stretching mode of NOR (Figure 3A, trace b) is located at 1930 $cm^{-1}$ and confirms the assignment of this mode. The frequency we detect is 4 $cm^{-1}$ higher than that observed in the RR experiments (*2*) and 3 $cm^{-1}$ lower than that observed in the light *minus* dark FTIR spectra under continuous light photolysis at −39 °C (*1*). Figure 2C shows the three forms of the CO-bound $aa_3$ enzyme at 1966 ($\alpha$-form), 1956 ($\beta$-form), and 1975 $cm^{-1}$ ($\gamma$-form). The frequency of the 1974 $cm^{-1}$ mode that we detect in NOR is very similar to the $\gamma$-form of the $aa_3$ enzyme (*22*) and to those observed in the $ba_3$ (*12*, *16*) and $caa_3$ (*17*) enzymes from *Thermus thermophilus*. The presence of a single peak at 1974 $cm^{-1}$ indicates that CO binds to heme $b_3$, as opposed to the majority of heme copper-oxidases, in a single conformation.

Figure 3B displays the $TRS^2$ FTIR difference spectrum of NOR at 5 $\mu$s after CO photolysis. The absence of a negative peak at 1974 $cm^{-1}$ demonstrates that full rebinding of CO has occurred at 5 $\mu$s. It should be noted that the experimental conditions (see Materials and Methods) used

in the TRS[2] FTIR experiment are very different to those of the TR[3] and previously reported flash photolysis experiments (*4*, *21*). Figure 2D shows the TRS[2]-FTIR difference spectra ($t_d$ = 5 $\mu$s to 50 ms, 8 $cm^{-1}$) of the fully reduced $aa_3$−CO complex from *P. denitrificans* after CO photolysis in $D_2O$. Under our experimental conditions (8 $cm^{-1}$ spectral resolution) the 1956, 1966, and 1975 $cm^{-1}$ peaks are not resolved, and thus a single negative peak is observed at 1966 $cm^{-1}$. The 4 $cm^{-1}$ resolution experiment (data not shown) clearly demonstrates the presence of the three bands, but the signal-to-noise is lower than that obtained with 8 $cm^{-1}$ resolution. The negative peak at 1966 $cm^{-1}$ arises from the photolyzed heme $a_3$−CO, and the intensity increase signals the onset of CO-rebinding to heme $a_3$. We do not detect the formation of the transient $Cu_B^{1+}$-CO complex ($\nu(Cu_BC-O)$ = 2061/2038 $cm^{-1}$) as it has been reported at low-temperature experiments (*24*). This indicates that the lifetime of the $Cu_B^{1+}$-CO complex is below our time-resolution of 5 $\mu$s, in agreement with previous work that reported a lifetime of 1 $\mu$s for the transient complex (*25*). The continuous variability in the intensity of the CO mode associated with heme $a_3$ is the most quantified aspect of ligand rebinding to heme $a_3$, and is depicted in the inset. The intensity of the $Fe^{2+}$-CO band shown in Figure 2D was measured as a function of time to determine the rate of CO recombination. The curve is a three-parameter fit to the experimental data according to first-order kinetics. The $k_{obs}$ = 50 $s^{-1}$ we have determined is similar to that previously reported by Woodruff and co-workers ($k_{obs}$ = 42 $s^{-1}$) in a review paper (*25*), and much smaller than that of NOR.

The insensitivity of the C−O mode that is associated with heme $b_3$ of NOR to H/D exchange argues against the possibility of H-bonding between the bound CO and residues within the distal pocket. Several factors can influence the strength of the C−O bond. For instance, distal effects involving the non-heme $Fe_B$ could alter the conformation of the Fe−C−O group from its preferred symmetry into a bent or tilt conformation thereby raising the C−O frequency. Also, the strength of the proximal histidine H-bonding interaction affects the strength of both the Fe−C and C−O bonds that can be further influenced by the $Fe_B$ distal environment. The Fe−His vibration of heme $b_3$ in NOR has a frequency at 207 $cm^{-1}$ and a C−O stretching mode at 1974 $cm^{-1}$ that are very similar to those found in cytochrome $ba_3$ (*12*, *26*). Notably, cytochrome $ba_3$ catalyzes the two-electron reduction of NO to $N_2O$ through the heme $a_3$−$Cu_B$ binuclear center (*5*), and we have recently reported the formation of the equilibrium $Cu_B^{1+}$-CO species as well as the rates of the decay of the transient $Cu_B$-CO complex (34.5 $s^{-1}$) and of the rebinding of CO to heme $a_3$ ($k_{obs}$ = 28.6 $s^{-1}$) (*12*, *16*). Despite the similarities associated with the strength of the Fe−His bond and the frequency of the bound CO to the heme in NOR and cytochrome $ba_3$, the difference in their ligand dynamics is significant. In the case of the $aa_3$ oxidase from *P. denitrificans*, the observation of the Fe−His and CO stretching frequencies at 220 and 1966 $cm^{-1}$ (*22*, *27*) in conjunction with the $k_{obs}$ = 50 $s^{-1}$ suggests that no structural or kinetic similarities are evident between NOR and $aa_3$ oxidase. Therefore, kinetic inferences cannot be drawn from structural analysis. On the surface it may seem surprising that the CO rebinding kinetics in NOR is faster than myoglobin, despite the presence of a non-heme Fe nearby to heme $b_3$. However, this is expected for the CO adducts in heme proteins when the photodissociated ligand is not migrated far away from the heme, in contrast to heme-copper oxidases CO adducts, since it has been demonstrated that the $Cu_B^{1+}$-CO adduct in heme-copper oxidases studied thus far is longed-lived ($\mu$s to ms).

The ligand binding/dynamics of the dinuclear center in NOR is a step toward the clarification of the catalytic mechanism and the rationalization of ligand kinetic behavior. Recent RR and optical studies (*3*, *21*) have suggested that NOR employs a P450-type mechanism, in which only heme $b_3$ functions as the NO binding site during turnover. In the mammalian $aa_3$ oxidase it has been suggested that binding of one molecule of NO to each metal center in the binuclear center of the fully reduced enzyme ($4e^-$) leads to oxidation of the heme as well as the nearby copper atom (*28*). This process involves the uptake of two protons and the generation of $N_2O$ and $H_2O$. However, we have recently reported the formation of six-coordinate ferric nitrosyl and five coordinate ferrous nitrosyl adducts of cytochrome $cbb_3$ oxidase and propose a mechanism for the NO reduction, in which NO binding occurs exclusively at the heme $b_3$ center (*29*, *30*). Although we have reported the formation of the nitrosyl heme $b_3$ species that can be real intermediates in the catalytic pathway, the mechanism of NO reduction to $N_2O$ by $cbb_3$ oxidase appears to be complex.

In summary, the comparative structural and kinetic data presented here suggest that although NorB is homologous to subunit I of the heme-copper oxidases and both enzymes reduce NO and $O_2$, their ligand dynamics is quite different. Establishing the structural and functional properties of the dinuclear center in NOR (heme $b_3$-$Fe_B$) and the binuclear center in cytochrome *c* oxidase (heme-$Cu_B$) are essential in understanding the linkage of the structural features with the structure of transient NO and $O_2$ intermediates that are important for the function of these proteins. Although the ligand dynamics of $Cu_B$ in heme-copper oxidases have been explored, the properties and the role of the non-heme $Fe_B$ in NOR remains unknown. The characterization of the functional/structural implications of the non-heme $Fe_B$ to heme $b_3$ pocket, will lead to a better understanding of the oxidative phase of NOR. These experiments are in progress in our laboratory.

## ACKNOWLEDGMENT

We thank Professor Bernd Ludwig for a kind gift of CcO from *P. denitrificans* and one of the reviewers for excellent suggestions.

## REFERENCES

1. Hendriks, J., Warne, A., Gohlke, U., Haltia, T., Ludovici, C., Lübben, M., and Saraste, M. (1998) *Biochemistry 37*, 13102−13109.
2. Moënne-Loccoz, P., and de Vries, S. (1998) *J. Am. Chem. Soc. 120*, 5147−5152.
3. Pinakoulaki, E., Gemeinhardt, S., Saraste, M., and Varotsis C. (2002) *J. Biol. Chem. 277*, 23407−23413.
4. Hendriks, J. H. M., Prior, L., Baker, A. R., Thomson, A. J., Saraste, M., and Watmough, N. J. (2001) *Biochemistry 40*, 13361−13369.
5. Giuffrè, A., Stubauer, G., Sart, P., Brunori, M., Zumft, W. G., Buse, G., and Soulimane, T. (1999) *Proc. Natl. Acad. Sci. U.S.A. 96*, 14718−14723.
6. Findsen, E. W., Centeno, J., Babcock, G. T., and Ondrias, M. R. (1986) *J. Am. Chem. Soc. 109*, 5367−5372.

7. Varotsis, C., and Babcock, G. T. (1995) *J. Am. Chem. Soc. 117*, 11260−11269.
8. Varotsis, C., and Babcock, G. T. (1993) *Methods Enzymol. 226*, 409−431.
9. Schelvis, H., Varotsis, C., Deinum, G., Ferguson-Miller, S., and Babcock, G. T. (1997) *J. Am. Chem. Soc. 119*, 8409−8416.
10. Varotsis, C., Kreszowski, D. H., and Babcock, G. T. (1996) *Biospectroscopy 2*, 331−338.
11. Rousseau, D. L. and Friedman, J. L. (1998) In *Biological Applications of Raman Spectroscopy* (Spiro, T. G., Ed.) Vol. 3, pp 133−215, John Wiley & Sons: New York.
12. Koutsoupakis, K., Stavrakis, S., Pinakoulaki, E., Soulimane, T., and Varotsis, C. (2002) *J. Biol. Chem. 277*, 32860−32866.
13. Dyer, R. B., Einarsdóttir, O., Killough, P. M., Lopez-Garriga, J. J., and Woodruff, W. H. (1989) *J. Am. Chem. Soc. 111*, 7657−7659.
14. Dyer, R. B., Peterson, K. A, Stoutland, P. O., and Woodruff, W. H. (1994) *Biochemistry 33*, 500−507.
15. Stavrakis, S., Koutsoupakis, K., Pinakoulaki, E., Urbani, A., Saraste, M., and Varotsis, C. (2002) *J. Am. Chem. Soc. 124*, 3814−3815.
16. Koutsoupakis, K., Soulimane, T., and Varotsis, C. (2003) *J. Biol. Chem. 278*, 14893−14896.
17. Pinakoulaki, E., Soulimane, T., and Varotsis, C. (2002) *J. Biol. Chem. 277*, 32866−32874.
18. Stavrov, S. (1993) *New J. Chem. 17*, 71−76.
19. Stavrov, S. (1993) *Biophys. J. 65*, 1942−1950.
20. Hendler, R. W., Pardhasaradhi, K., Reynafarje, B., and Ludwig, B. (1991) *Biophys. J. 60*, 415−423.
21. Hendriks, J. H. M., Jasaitis, A., Saraste, M., and Verkhovsky, M. I. (2002) *Biochemistry 41*, 2331−2340.
22. Pinakoulaki, E., Pfitzner, U., Ludwig, B., and Varotsis, C. (2002) *J. Biol. Chem. 277*, 13563−13568.
23. Kitagawa, T. (1998) in *Biological Applications of Raman Spectroscopy* (Spiro, T. G., Ed.) Vol. 3, pp 97−131, John Wiley & Sons: New York.
24. Rost, B., Behr, J., Hellwig, P., Richter, O.-M. H., Ludwig, B., Michel, H., Mäntele, W. (1999) *Biochemistry 38*, 7565−7571.
25. Woodruff, W. H. (1993) *J. Bioenerg. Biomembr. 25*, 177−188.
26. Oertling, W. A., Surerus, K. K., Einarsdóttir, O., Fee, J. A. Dyer, R. B., Woodruff, W. H. (1994) *Biochemistry 33*, 3128−3141.
27. Pinakoulaki, E., Pfitzner, U., Ludwig, B., and Varotsis, C. (2003) *J. Biol. Chem. 278*, 18761−18766.
28. Rousseau, D. L., Singh, S., Ching, Y-c., and Sassaroli, M. (1988) *J. Biol. Chem. 263*, 5681−5685.
29. Stavrakis, S., Pinakoulaki, E., Urbani, A., and Varotsis, C. (2002) *J. Phys. Chem. B 106*, 12860−12862.
30. Pinakoulaki, E., Stavrakis, S., Urbani, A., and Varotsis C. (2002) *J. Am. Chem. Soc. 124*, 9378−9379.

BI035289M